Chapter 10

Synthesis, Characterization and Properties of Zirconium Oxide (ZrO_2)-Doped Titanium Oxide (TiO_2) Thin Films Obtained via Sol-Gel Process

Rabah Bensaha and Hanene Bensouyad

Additional information is available at the end of the chapter

http://dx.doi.org/10.5772/51155

1. Introduction

Sol–gel process [1-3] is an attractive alternative to other methods for synthesis of ceramics and glasses for many reasons: for example, low temperature synthesis, simple equipment's to be used, thin film formability and so on. Particularly, sol–gel process is very useful for thin film deposition because of the capability to coat materials of various shapes and/or large area, to control the composition easily for obtaining solutions of homogeneity and controlled concentration without using expensive equipment.

Historically, metal alkoxides have been employed in sol–gel process, which readily undergo catalyzed hydrolysis and condensation to form nanoscale oxide or hydroxide particles. Still in general, metal alkoxides are often used as raw materials in sol–gel process, but many of the alkoxides are very difficult to be obtained because of the high sensitivity to the atmospheric moisture [4-9]. In ordinary sol–gel processing, starting compositions as well as reaction conditions are selected so as to maintain the mixture in a homogeneous state throughout the processes including mixing of starting compounds, gelation, aging, drying and heat-treatment.

Titanium and zirconium oxides are very promising candidates for future technology of thin layers because of their interesting mechanical, thermal and chemical properties. Titanium oxide (TiO_2) is a cheap, non-toxic, and non-biodegradable material, besides their widely uses in various industries [10]. Moreover, it is a semiconductor under the form of thin films. Its insensitivity to visible light due to its band gap (3.2 eV) enables it to absorb in the near ultraviolet region [11], even though its low efficiency. Hence, it can be sensitized by a great number of dyes; some of them allow a conversion rate incident photon–electron approaching unity. Thus, these various applications arouse great interest in the study of

titanium oxide thin films. The significant uses of TiO_2 thin films are in solar cells [12], photo-catalytic [13] and electro-chromic systems [14], in other words, they are mainly found their use in optics.

TiO_2 thin films are extensively studied because of their interesting chemical, electrical and optical properties [15,16]. TiO_2 film in anatase phase could accomplish the photocatalytic degradation of organic compounds under the radiation of UV. So, it has a variety of application prospects in the field of environmental protection [17,18]. TiO_2 thin film in rutile phase is known as a good blood compatibility material and can be used as artificial heart valves [19]. In addition, TiO_2 films are important optical films due to their high reflective index and transparency over a wide spectral range [16].

During the two last decades, several methods have been used for the TiO_2 thin films preparation, such as chemical vapor deposition [20], chemical spray pyrolysis [21], pulsed laser deposition [22] and sol–gel method [23]. In comparison with other methods, the sol–gel method has some advantages such as controllability, reliability, reproducibility and can be selected for the preparation of nano-structured thin films [23,24]. Sol–gel coating has been classified as two different methods such as dip and spin coating.

The dip-coating has considerably been used for preparation TiO_2 nanostructured thin films [25–27]. Experimental results have shown that the preparation of high transparent TiO_2 thin film by dip-coating method needs to control morphology, thickness of the film and the anatase-brookite-rutile phase transformation [26,28].

Additions of another semiconductor have been used to improve the properties of titanium dioxide. In principle, the coupling of different semiconductor oxides seems useful in order to achieve a higher photocatalytic activity [29]. Various composites formed by TiO_2 and other inorganic oxides such as SiO_2 [30], ZrO_2 [31] SnO_2 [32], Cu_2O [33], MgO [34], WO_3 [35], In_2O_3 [36], ZnO [37], MoO_3 [38], CdS [39], PbS [40], and so on, have been reported.

Zirconium oxide (ZrO_2) has good dielectric and optical properties [41,42] it has a high refraction index [43]. Additionally, it has a very good transparency on a broad spectral field [44], a great chemical stability and a threshold of resistance to high laser flow. All these properties led to miscellaneous applications such as optical filters, laser mirrors [45] or barriers layers from the heat [46]. ZrO_2 films are also employed as plug layer for super-conducting ceramics [47,48], like biomaterial for prostheses [49,50], as gas sensor [51] or like component in combustible batteries [52]. Basically, ZrO_2 itself is an insulating direct wide gap metal oxide, with an optical band gap in the range 5.0-5.85 eV [53].

The aim of the present work is to investigate the transformation behaviors and the effect; of a smaller ratio range of ZrO_2; doping on the surface area of TiO_2 thin films, light absorption, band gap energy, variations of crystal granularity, phase composition and especially on the evolution of the crystallite size and defects concentration with annealing treatments (heat treatments) and layers thickness of the samples produced. So that in this chapter, we report the study of structural, thermal and optical properties of ZrO_2-doped TiO_2 thin films deposited by the sol–gel process. Several experimental techniques were used to characterize

structural and optical properties resulting from different annealing treatments and different layer thicknesses: X-ray powder diffraction, Fourier transforms infrared (FTIR), Raman spectroscopy, Scanning electron microscopy (SEM), differential scanning calorimetric (DSC), Scanning electron microscopy (SEM), the energy dispersive X-ray spectrometry (EDX) and UV spectroscopy.

To obtain nanomaterial's with controlled properties, it is most often involves the use of mineral additives (dyes, semiconductors, metal particles, rare earth, etc.) in small quantities. These additions can promote densification or control the phenomenon of grain growth, or to change the structural, physical and optical properties. So the presence of impurities in a matrix can stabilize, improve or modify the various properties of a material. Generally, thin layers of doped TiO_2 give hope of significant performance gains and new applications.

2. Experiments

Our 5% ZrO_2-doped TiO_2, thin films were prepared by dip coating, in three steps. The first step: the dissolution of 1 mol of butanol (C_4H_9OH) as solvent, 4 mol of acetic acid ($C_2H_4O_2$), 1mol of distilled water and 1 mol of tetrabutylorthotitanate $(C_4H_9O)_4Ti$. In the second step, the solution of ZrO_2 was prepared from the dissolution of 1 mol of zirconium oxychloride salt ($ZrOCl_2 \bullet 8H_2O$) in distilled water and 2 mol of ethanol (95%) as catalyst. Finally, the solution of TiO_2 was doped with ZrO_2. Then, the resultant yellowish transparent solutions were ready for use. The substrates were dip-coated in the solutions at a constant rate of 6.25 cm.s-1. After each dipping, thin films were dried for 30 min at a distance of 40 cm from a 500 W light source. The drying temperature of the light source is approximately equal to 100 °C. Subsequently, thin films were heat treated in the temperature range 350–450 °C, with a temperature increase rate of $5°C.min^{-1}$, for 2 h in the furnace. The powders obtained from the xerogel were prepared in room temperature and under air atmosphere.

After each dipping, the thin films were dried for 30 min, at a distance of 40 cm from a 500 Wight source. The drying temperature of the light source is approximately equal to 100 °C. Subsequently, thin films were heat treated in the temperature range 350–450 °C, with a temperature increase rate of 5 °C min^{-1}, for 2 h in the furnace. The powders obtained from the xerogel were prepared with an annealing till three months in room temperature and under air atmosphere.

To investigate the transformation behaviors and the effect; of a smaller ratio range of ZrO_2; doping on the surface area of TiO_2 thin films, light absorption, band gap energy, variations of crystal granularity, phase composition and especially on the evolution of the crystallite size and defects concentration with annealing treatments (heat treatments) and layers thickness of the samples produced.

So that in this chapter, we report the study of structural, thermal and optical properties of ZrO_2-doped TiO_2 thin films deposited by the sol–gel process.

Several experimental techniques were used to characterize structural and optical properties resulting from different annealing treatments and different layer thicknesses: X-ray powder

and films diffraction, Fourier transforms infrared (FTIR), Scanning electron microscopy (SEM), Raman spectroscopy, differential scanning calorimetric (DSC), Scanning electron microscopy (SEM), the energy dispersive X-ray spectrometry (EDX) and UV spectroscopy.

To determine the transformation points, the obtained powdered xerogels were analyzed by Differential Scanning Calorimetry (DSC) using a SETARAM DSC–92 analyzer equipped with a processor and a measuring cell. The thermal cycle applied consists of heating from room temperature to 520°C, holding for 5min at this temperature and finally cooling back to room temperature with the same rate (5°C/min). X-ray powder diffraction was performed by Siemens D5005 diffractometer using a Cu $K_{\alpha 1}$ radiation. The patterns were scanned at room temperature, over the angular range 10-70° 2θ, with a step length of 0.1° 2θ and counting time of 1 s.step^{-1}. The UV absorption studies were carried out using UV-VIS double–beam spectrophotometer SHIMADZU (UV3101PC). Its useful range is between 190 and 3200 nm. The treatment of the spectra was performed using the UVPC software. A surface profiler DEKTAK 3ST AUTO1 (VEECO) was used to determine film thicknesses. Raman spectra were recorded in a back scattering configuration with a Jobbin Yvon micro Raman spectrometer coupled to a DX40 Olympus microscope. The samples of doped and undoped TiO_2 thin films were excited with a 632.8 nm wavelength with an output of 20 mw.

3. Results

3.1. Solution properties

3.1.1. Viscosity

This part is devoted to study the effect of solution aging and its viscosity on the films thickness. To do this study, five samples are developed, successively on the day, the next day, after seven days, after 10 days, and after fourteen days of solution synthesis. The conservation of the sol during the 14 days is made at room temperature.

Table 1 shows an important change of layers thickness with the increasing of the solution viscosity. After a repose period of 14 days of synthesis solution doped with ZrO_2, the thickness of layer changes from 32 nm, with a viscosity 10 mPa.s, to 81 nm when the viscosity is 180 mPa.s. We notice that the ZrO_2-doped TiO_2 solution becomes more viscous over time (Figure 1). This reflects the rate of polycondensation reaction progress.

solution age	η (mPa.s)	Measured thicknesses d (nm)
0 day	10	32
1 day	20	33
7 days	60	39
10 days	110	61
14 days	180	81

Table 1. Variation of film thicknesses d (nm) with solution viscosity.

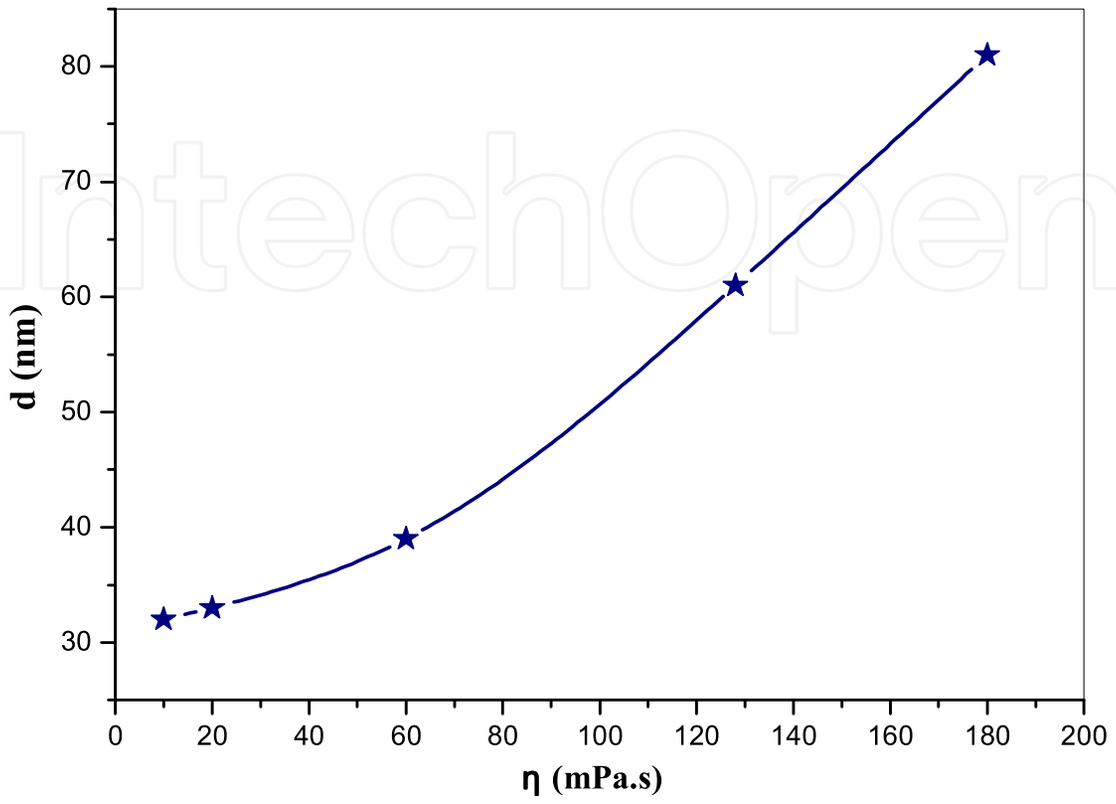

Figure 1. Variation of film thicknesses d (nm) with solution viscosity η(mPas.s)

3.2. Powder Properties (Xerogel)

3.2.1. X-Ray Diffraction (XRD)

Figure 2a and b shows the X-ray diffraction (XRD) patterns of TiO_2 xerogels of undoped (Figure 2a) and 5% ZrO_2-doped TiO_2 (Figure 2b). The XRD pattern evolution of titanium xerogel obtained after the evaporation of the organic compounds during 3 months of aging at ambient temperature shows that it is an amorphous phase as reported in [54].

It has been reported that the used acid catalyst, during sol–gel preparation, plays a crucial role for determining the TiO_2 phase, in literature [54, 55], they found that powder is amorphous when they use acetic acid as catalyst. However, when using formic acid they found that, in addition to amorphous phase, there is an amount of the anatase nanoparticles. This analysis of the doped TiO_2 xerogel exhibits that the addition of 5% ZrO_2 (Figure 2b) would be largely sufficient to form nanoparticles of anatase which crystallizes with (101) plane. It is interesting to note that the addition of a minor amount of ZrO_2 starts crystallization of anatase. Whereas, A. Kitiyanan et al. [56] B. Neppolian et al. [57] reported that addition of ZrO_2 has no effect on TiO_2 oxide morphology..

3.2.2. Thermal analysis

The differential scanning calorimetric (DSC) curves of undoped TiO_2 and 5% ZrO_2-doped TiO_2 xerogels are shown in Figure 3 It is interesting to note that both doped and undoped xerogels showed a similar thermal behavior in the temperature range 20–250 °C. Generally, weight loss corresponds to the evaporation of water, thermal decomposition of butanol as well as carbonization or combustion of acetic acid and other organic compounds [58-60] which constitute metal alkoxides. Hence, the above thermal events were represented by an endothermic peak spreading from 50 to 250 °C.

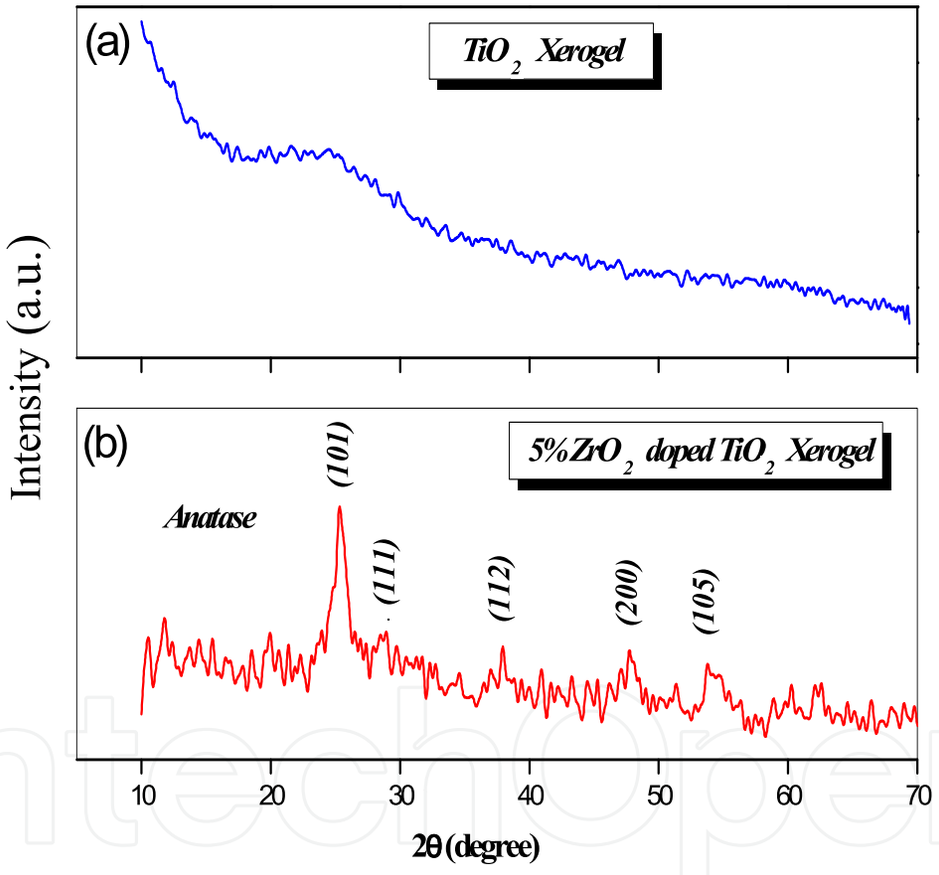

Figure 2. Evolution of XRD patterns of xerogels (a) undoped TiO_2, and (b) 5% ZrO_2-doped TiO_2.

A double exothermic peak in the 260–450 °C temperature range of TiO_2 xerogel can be attributed to the crystallization of titanium oxide [61].

The addition of 5% of zirconium oxide led to a shift of exothermic peak phase towards lower temperatures. This may be due to the speeding up of the crystallization of titanium oxide compared to the undoped one.

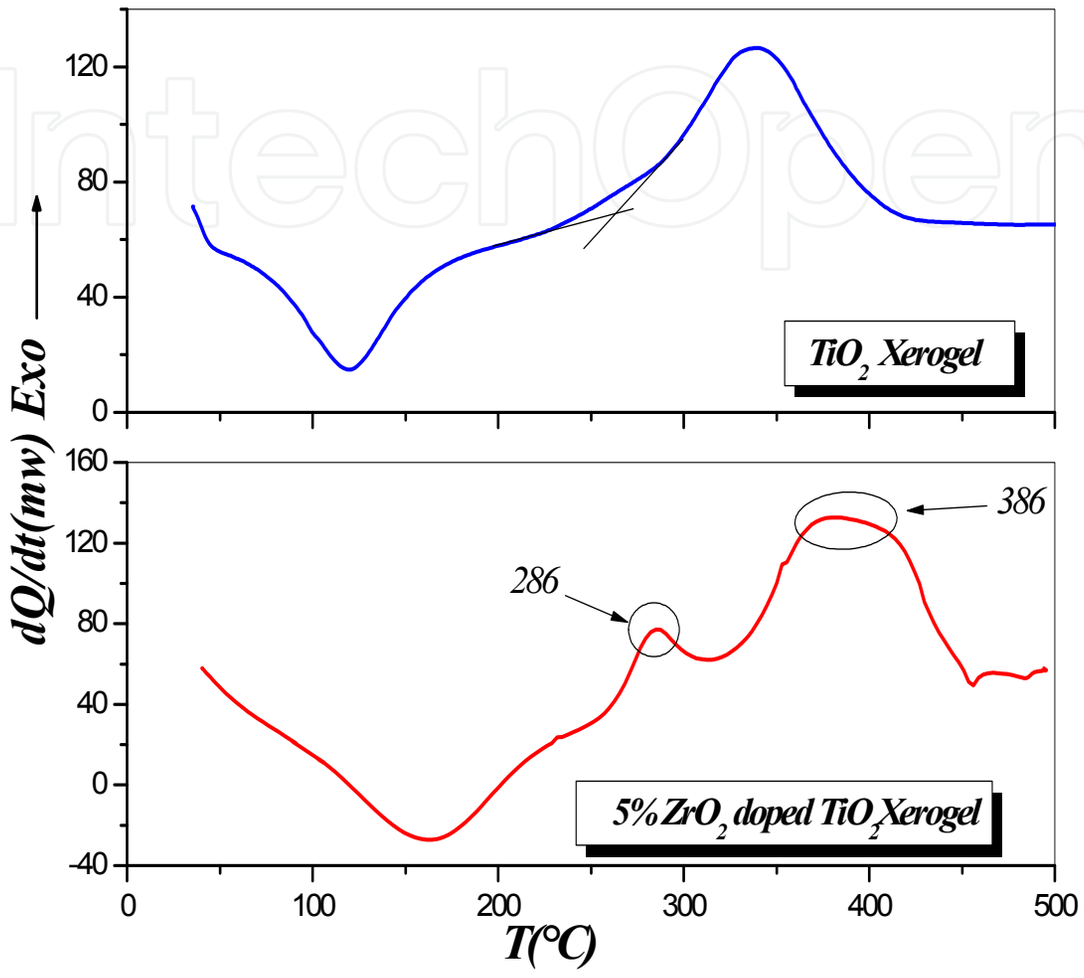

Figure 3. Differential scanning calorimetric curves of xerogels: (a) undoped TiO_2 and (b) 5 % ZrO_2-doped TiO_2.

3.3. Thin films properties

3.3.1. Structural Properties

3.3.1.1. Thin films thickness

The measured values of thin films thickness, given in Figure 4, were determined with a surface profiler for various layers and at different annealing temperatures. It is clearly observed that the film thickness increases with the number of dipping and annealing temperatures.

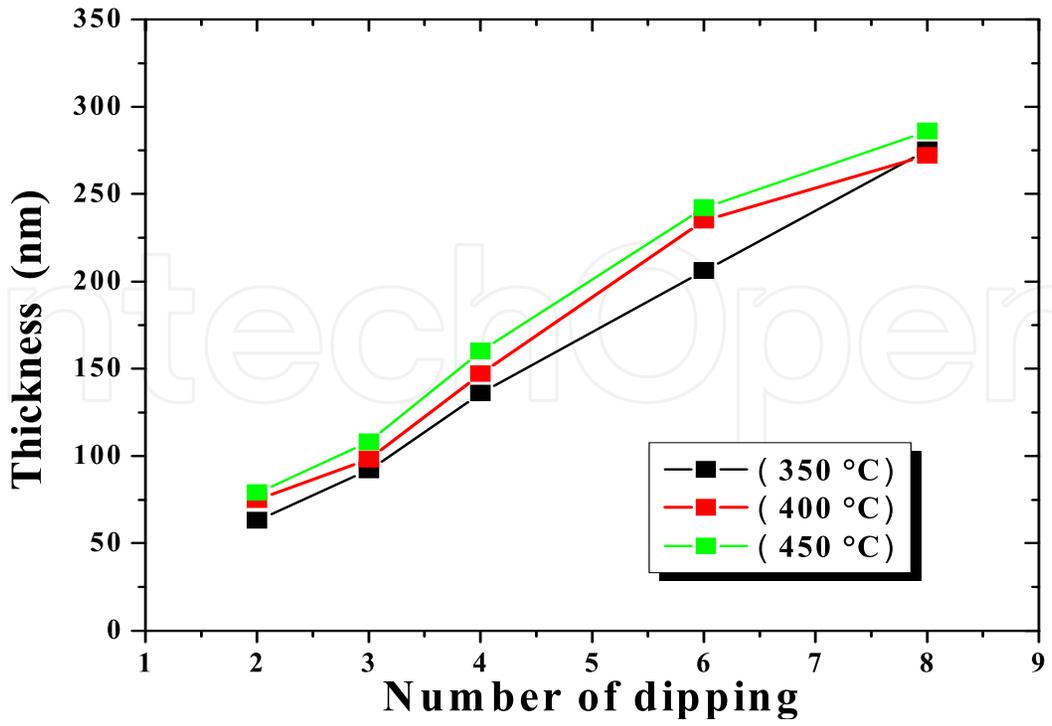

Figure 4. Variation of film thicknesses d (nm) for different annealing temperatures and different dipping

3.3.1.2. Study of deposition rate

A thin film deposited by dip-coating method has a thickness which can be controlled by the deposition rate. To simplify, d thickness depends on the speed according to the following relationship:

$$d = k.V_d^{\ a}$$

Where:

V_d is the deposition rate, k is the empirical factor depending on the viscosity, surface tension and density of the solution used and a is the exponent with 2/3 value according to Landau and Levich [62], and 1/2 according to Michels et al. [63] or even proportionately at the speed of dipping Hewak et al. [64].

We then set the objective of determining this factor to validate one of these different models. So, we have prepared six samples with different deposition rate from 0.6 $cm.s^{-1}$ to 2 $cm.s^{-1}$ in the same conditions (deposited in solution with a viscosity 40 mPa.s at 21°C and treated at 400°C); we measured their thicknesses by profilometer and the results are grouped in table 2 and represented in figure 5.

This curve shows a linear increase in ln(d) versus ln(V_d). For the exponent a, values of 0,965 have been obtained, which is in good agreement with the exponent obtained by Hewak et al. [64]. This simple comparison shows that the increase in the speed of dipping, results an increase in the thickness of doped thin films.

Deposition rate (cm.s^{-1})	0.6	0.8	1	1.4	1.8	2
Thickness (± 0.1 nm)	38	56	74	93	116	143

Table 2. Variation of film thickness d (nm) for different deposition rate.

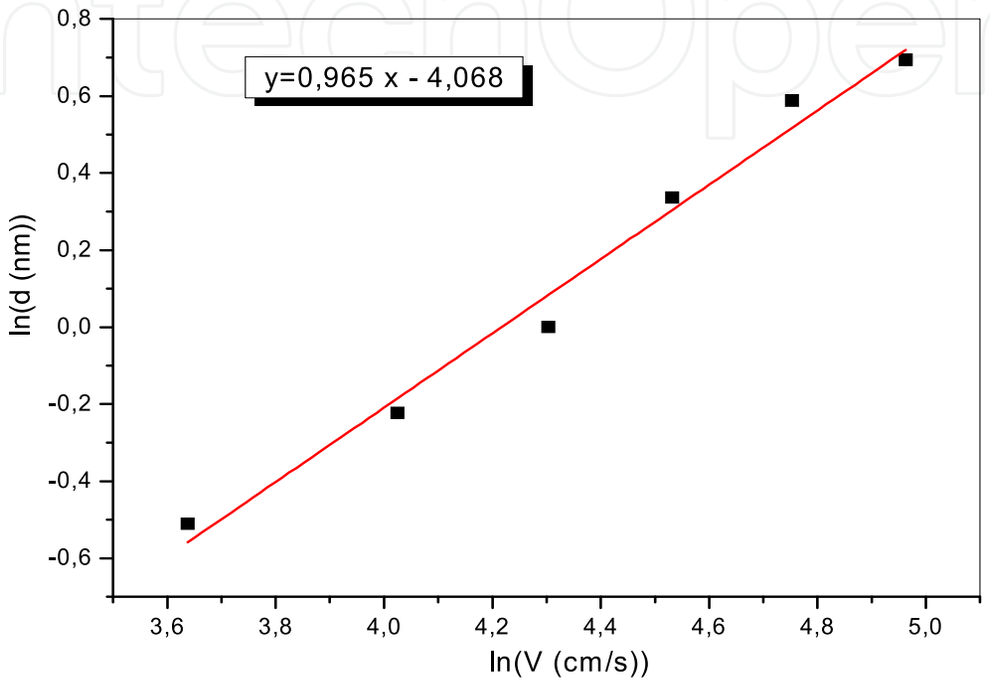

Figure 5. Variation of thickness logarithm with deposition rate logarithm.

3.3.1.3. X-Ray Diffraction (XRD)

3.3.1.3.1. Crystallization

a. Influence of annealing temperature

Our samples were analyzed using X-ray diffraction (XRD) to investigate the transformation behaviors. We have studied the structural properties of undoped TiO_2, and doped with 5% ZrO_2 thin films and deposited by the sol–gel method. The dip-coated thin films have been examined at different annealing temperatures (350 to 450 °C).

Figure 6 shows XRD patterns of 5% ZrO_2-doped TiO_2 thin film obtained after different dipping and treated at 450 °C. However, Figure 7 shows XRD patterns of 5% ZrO_2-doped TiO_2 thin film obtained after 2 dipping and treated at various annealing temperatures at 350 °C, 400 °C and 450 °C. Clearly, titanium oxide starts to crystallize starting from annealing at 350 °C.

This analysis of the doped TiO_2 thin films exhibits that the addition of a minor amount of ZrO_2 would be largely sufficient to form 4 sharp diffraction peaks at 25.35°, 35.51°, 50.90°

and 60.76°, these are assigned to (101), (112), (200), and (105) planes which are attributed to anatase nanoparticles (crystalline) phase of TiO_2.

Furthermore, all XRD patterns show a peak at 30.41° corresponding to (111) plane which is attributed to the brookite formation whatever the annealing temperature.

Peak intensities corresponding to characteristic planes of anatase (101) and brookite (111) phases are obviously increased with the increase of annealing temperature and number of dipping. This latter is interpreted as due not only to increase in proportion of titanium oxide but also to the improvement of the crystalline quality.

However, in the same conditions Kitiyanan et *al.* [56] B. Neppolian et *al.* [57] showed that titanium oxide, crystallizes in anatase phases and they found that addition of minor amount of ZrO_2 has not contributed to any change in the TiO_2 morphology.

b. Influence of doping with ZrO_2

Comparison between XRD patterns (Figure 8) of both undoped and doped with 5% ZrO_2 thin films obtained after 2 dippings and annealed at 400 °C temperature showed a similar behavior, so characteristic peaks correspond to the crystallization of anatase and brookite phases of the doped state is shifted to larger angles compared to the undoped one.

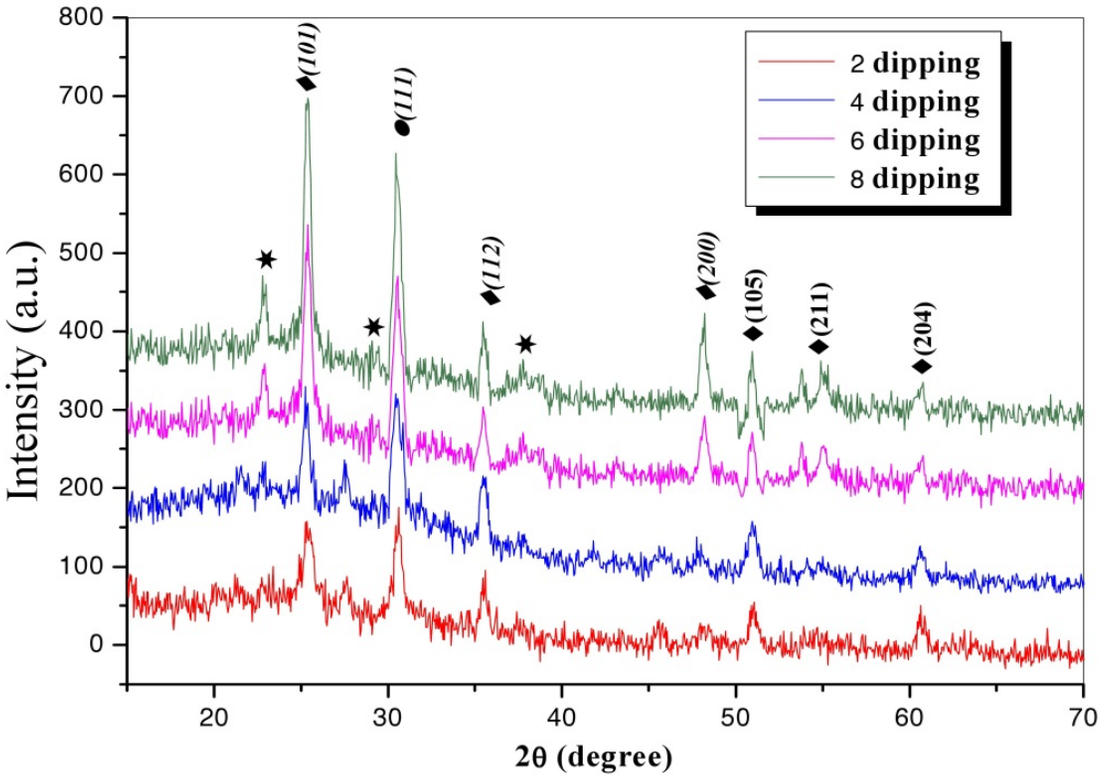

Figure 6. Evolution of diffraction patterns of 5% ZrO_2-doped TiO_2 thin films; obtained after various dipping (2, 4, 6, 8) annealed at 450°C. ★: substrat, ♦: anatase, ●: brookite.

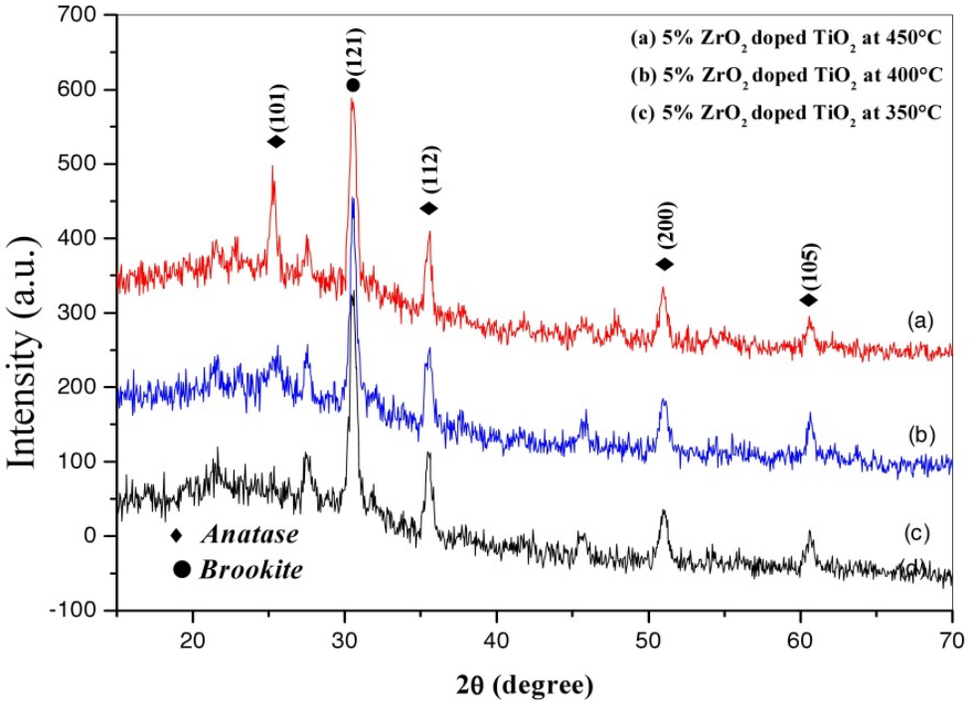

Figure 7. Evolution of diffraction patterns of 5% ZrO_2-doped TiO_2 thin films; obtained at various annealing temperatures (350, 400, 450 °C) for the same thickness.

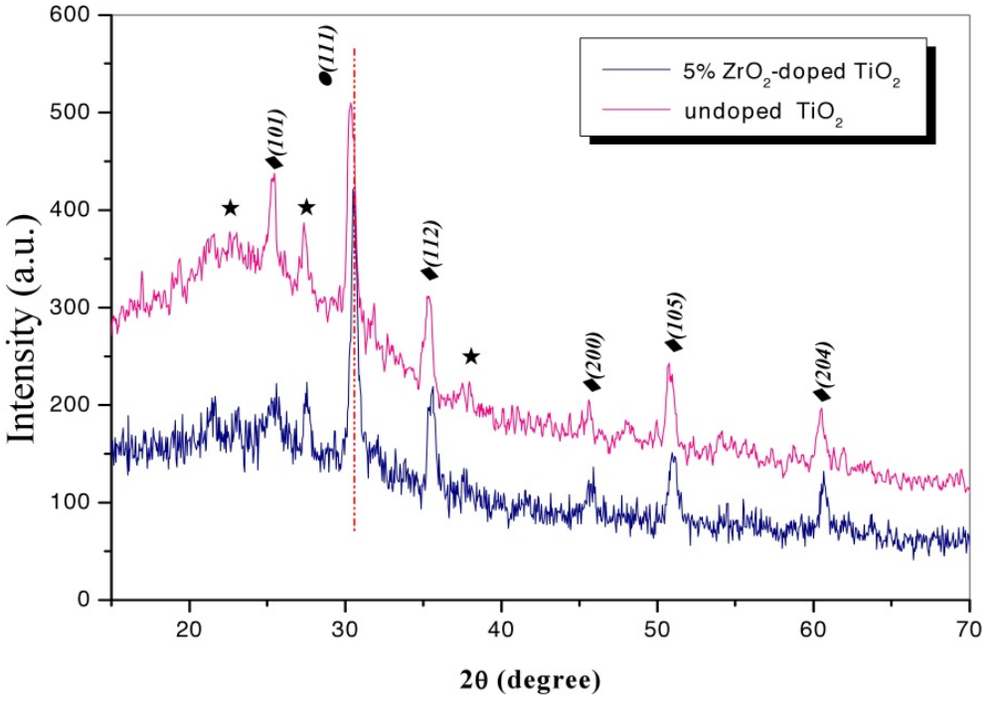

Figure 8. Comparison between undoped and 5% ZrO_2-doped TiO_2 diffraction patterns.

3.3.1.3.2. Surface morphology and grain size

The crystallite size D of TiO_2 doped with ZrO_2 thin films can be deduced from XRD line broadening using Scherrer equation [65]:

$$D = \frac{0.94 \times \lambda}{\sqrt{\left(\Delta_{hkl}^2 - \Delta_{instr}^2\right)}} \frac{1}{\cos\theta}$$

λ is the wavelength of X-ray beam (Cu K_α=1.5406 Å), Δ_{hkl} is the full width at half maximum (FWHM) of (hkl) diffraction peak, Δ_{instr} is the FWHM corresponding to the instrumental limit, and θ is the Bragg angle.

Using the size of the crystallites, the dislocation density (δ) [66], the number of crystallites per unit surface area (N) and strain in the films (ε), which are newly introduced by Ray et al. [66], has been determined:

$$\delta = \frac{1}{D^2}$$

$$N = \frac{d}{D^3}$$

$$\varepsilon = \frac{\Delta(2\theta) \cdot \cos\theta}{4}$$

Where d is the film thickness.

The calculated structural parameters are presented in Table 3.

		Annealed at	Phase	(hkl)	L (nm)	δ (10^{-4} traits/nm^2)	N (10^{-3} nm^{-2})	ε (10-4)
Undoped TiO_2	Xerogel	3 months at T ambient	Amorphous	-	-	-	-	-
5 %ZrO_2-doped TiO_2	Xerogel	3 months at T ambient	Anatase	(101)	14,80	-	-	-
	Same thickness	350 °C	Anatase	(101)	8,58	135,84	99,74	3,11
			Brookite	(111)	17,50	32,65	11,76	3,89
			Anatase	(112)	16,66	36,03	13,62	4,52
			Anatase	(200)	14,74	46,03	19,67	6,69
			Anatase	(105)	16,33	37,50	14,47	7,53
		400 °C	Anatase	(101)	10,09	98,22	73,01	3,07
			Brookite	(111)	17,61	32,25	13,73	3,82
			Anatase	(112)	17,27	33,53	14,56	4,44
			Anatase	(200)	15,57	41,25	19,87	6,37
			Anatase	(105)	18,71	28,57	11,45	7,58
		450 °C	Anatase	(101)	13,92	51,61	29,29	2,98
			Brookite	(111)	18,06	30,66	13,41	3,74
			Anatase	(112)	19,09	27,44	11,36	4,38
			Anatase	(200)	18,63	28,81	12,22	6,34
			Anatase	(105)	20,56	23,66	9,09	7,47

Table 3. Structural parameters of xerogels and thin films, for different annealing temperatures and same thickness.

The computed values of grain sizes, given in Table 3, were calculated for different annealing temperatures with the same thickness. Thus, the obtained grain sizes of anatase and brookite increase from 8.58 nm to 20.56 nm and from 17.50 nm to 18.06 nm, respectively. In fact, as annealing temperature increases grain sizes also increases.

It is interesting to note that the grain size improves and the defects like dislocation density and strain in the films decrease with film thickness. This may be due to the improvement in crystallinity in the films with film thickness. As we also note that the variation of the strain is perfectly correlated with that of the dislocation density δ. When these increase, they cause the decrease in grain size and leads to recrystallization of the nanoparticles. Furthermore, the stages of nucleation, growth and coalescence become stable, which causing the reduction of constraints in the film formed.

The evolution of the grain size D according the annealing temperature can be interpreted by the Arrhenius law (figure 9):

$$D = D_0 exp\left(-E_a / k_b T\right),$$

Where:

- E_a is the energy activation of crystallization;
- K_B the Boltzmann constant;
- D_0 pre-exponential factor.
- The size D tends towards the infinite for high temperatures [67].

The values of activation energies of crystallization corresponding respectively to anatase and brookite phases are calculated from the curve showed in figure 9, we note that the activation energy of the anatase E_a=0,096 eV crystallization is lower than that of the brookite E_a=0,012 eV. This means that the formation of anatase requires more energy than that of brookite.

3.3.1.4. RAMAN

The Raman spectra of undoped and 5% ZrO_2-doped TiO_2 thin films annealed at 450°C for different dipping (figure 10) display various peaks related to titanium oxide as anatase and brookite phases. These spectra exhibit bands at around 138 (strong), 235 (weak), 514 (weak) and 632 cm-1 (medium)) for the thin layers of ZrO_2-doped TiO_2 corresponding to the Eg modes of vibration. The above bands can be assigned to anatase phase except the band 235 cm^{-1} corresponding to the B_{1g} modes of vibration, which is due to the crystallization of brookite phase. While bands of 144, 188 and 651 cm-1 can be assigned to both anatase and brookite phases [68,69].

A slight shift of the most intense peak, Eg, to smaller wavenumber is observed for all thin films doped with ZrO_2 by comparison with anatase of undoped phase (figure 11). Similar displacements have been previously reported in XRD patterns and they can be correlated with the confinement effects in nano-structured anatase crystallites.

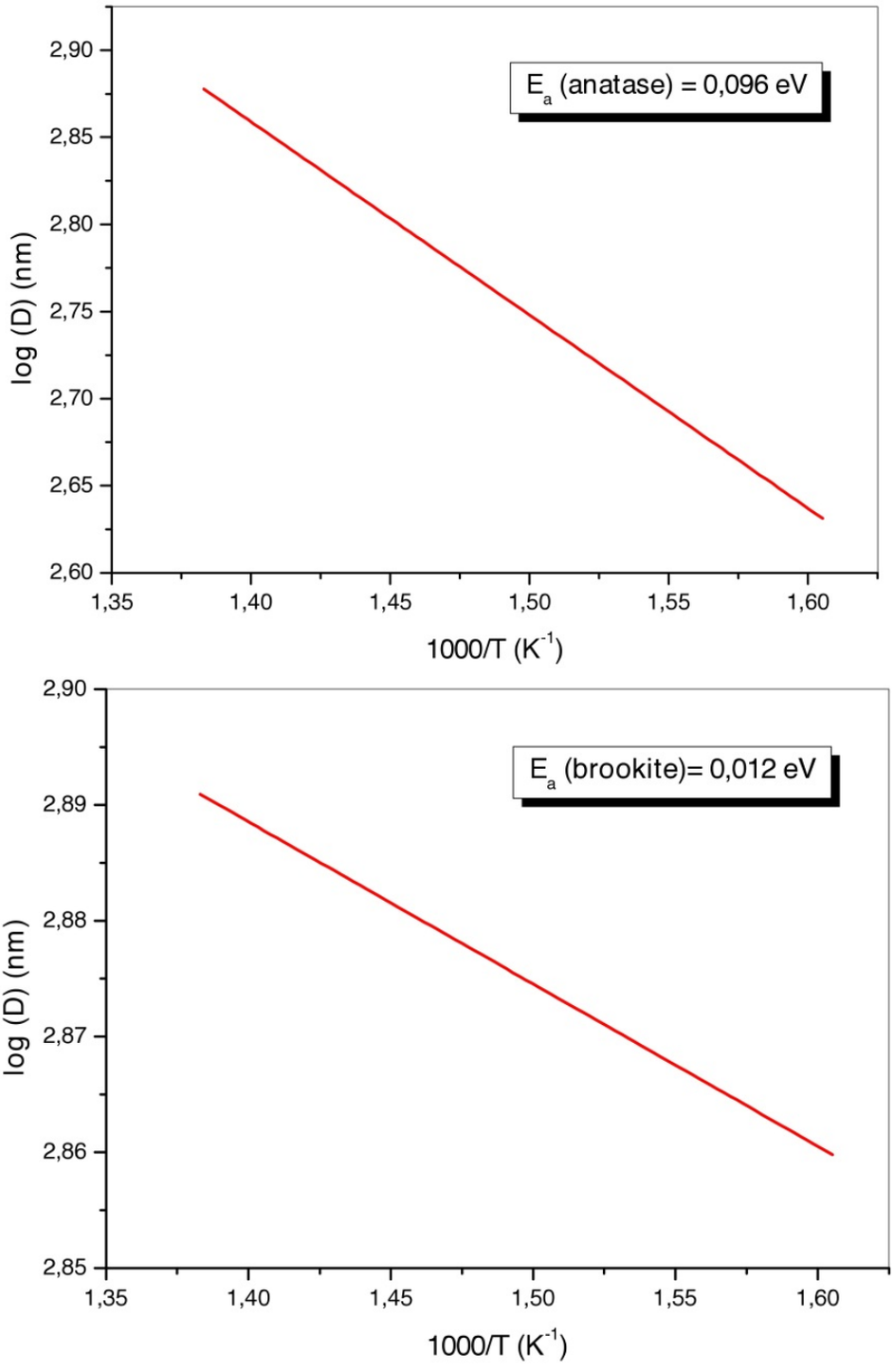

Figure 9. Plot of log (D) versus (1000/T) for determination of activation energies of anatase and brookite

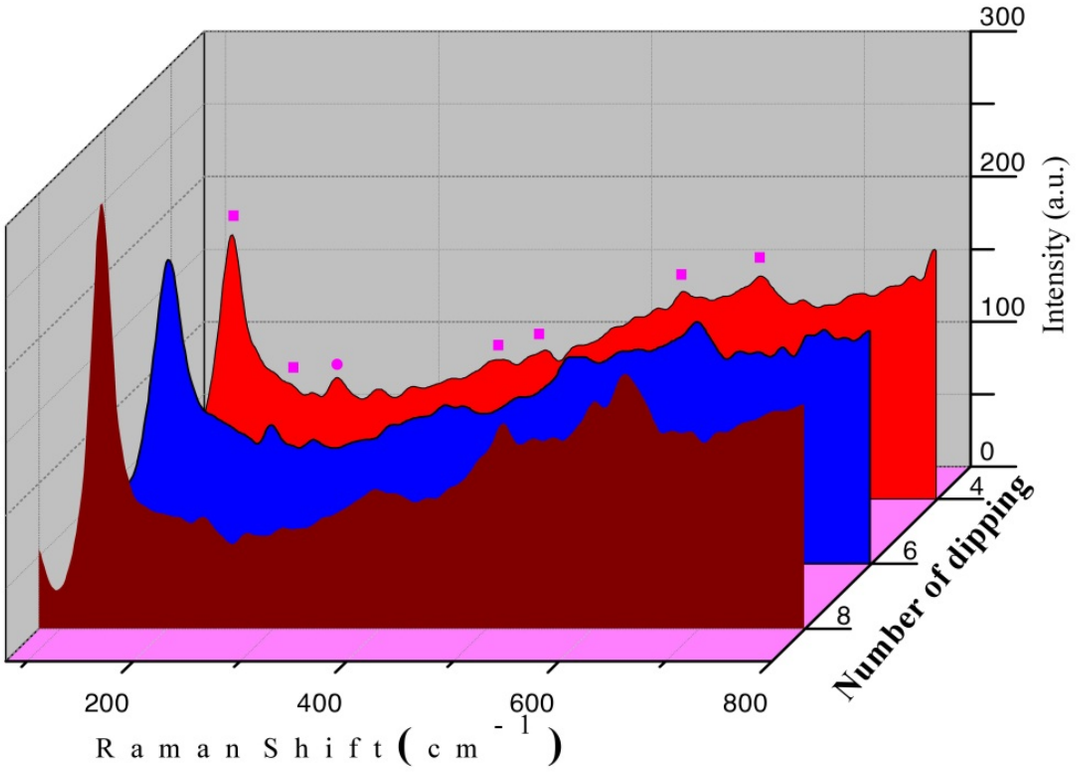

Figure 10. Raman spectrum of 5% ZrO_2-doped TiO_2 thin films annealed at 450°C for different dipping; ■=anatase, •=brookite.

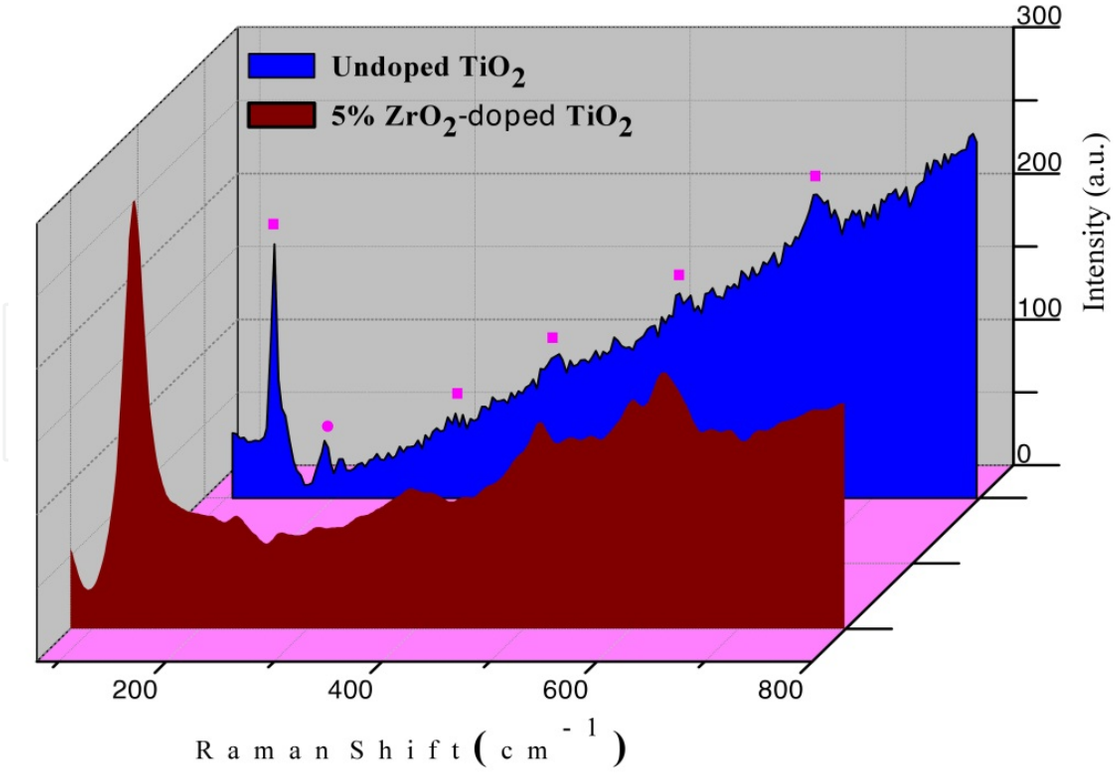

Figure 11. Comparison between Raman spectrum of undoped and 5% ZrO_2-doped TiO_2 thin films; ■=anatase, •=brookite.

3.3.1.5. FTIR

Figure 12 shows the infrared absorption spectrum of the 5% ZrO_2 -doped TiO_2 films annealed at different temperature. The peak at 2360 cm^{-1} resulted from the adsorbed H_2O molecules, which were not removed completely after sol–gel coating. The peaks at 1242 cm^{-1}, 1111 cm^{-1}, 1035 cm^{-1} and 860 cm^{-1} correspond to the vibration mode of Ti-OH [70, 71].

The band around 665 cm^{-1} was attributed to the vibration mode of Ti-O-Ti bond [72] and another bond appears around 455 cm^{-1}, this is the O-Ti-O band corresponding to the crystalline titania in the anatase form [73-76].

We find that the vibration bands intensity located in the vicinity of 665 cm^{-1} and 455 cm^{-1} increase when annealing temperature increases. This indicates that the number of Ti-O-Ti and O-Ti-O links of titanium dioxide crystallization is also growing.

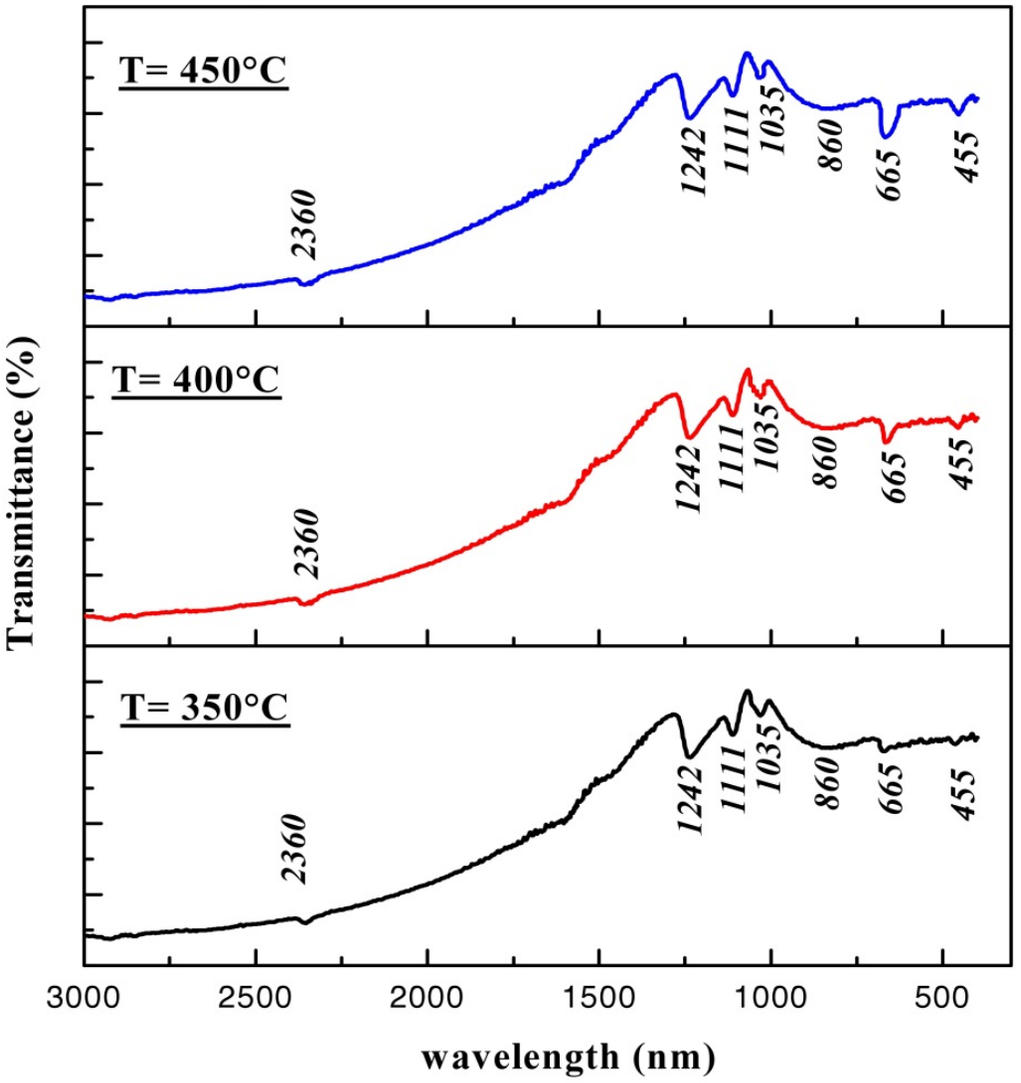

Figure 12. FTIR spectra of 5% ZrO_2-doped TiO_2 thin films, obtained at various annealing temperatures (350, 400, 450 °C).

3.3.1.6. Scanning electron microscopy (SEM) and EDX

5% ZrO_2-doped TiO_2 thin films deposited on ITO substrates and obtained after various annealing temperature at 350°C and 450°C were coated and examined in a scanning electron microscope (SEM) to investigate their structure and surface characteristics. We observed that the coating was homogeneous without any visual cracking over a wide area. The increase in the treatment temperature, did not affect the uniformity of the film.

The surface composition of films is further identified by EDX measurement. EDX result shown in Figure 13 demonstrates that the peaks of Ti, O and Zr can be clearly seen in the survey spectrum. While the other elements as Si, In, Ca, Na and Mg are the components of ITO substrate.

The chemical compositions of thin film analyzed are given in table 4.

	O	Na	Mg	Si	Ca	In	Zr	Ti	Total
at.%	40,13	2,03	3,15	37,83	3,07	4,39	1,23	8,17	100

Table 4. Elemental composition (at. %) of 5% ZrO_2 -doped TiO_2 thin films, treated at 450 ° C.

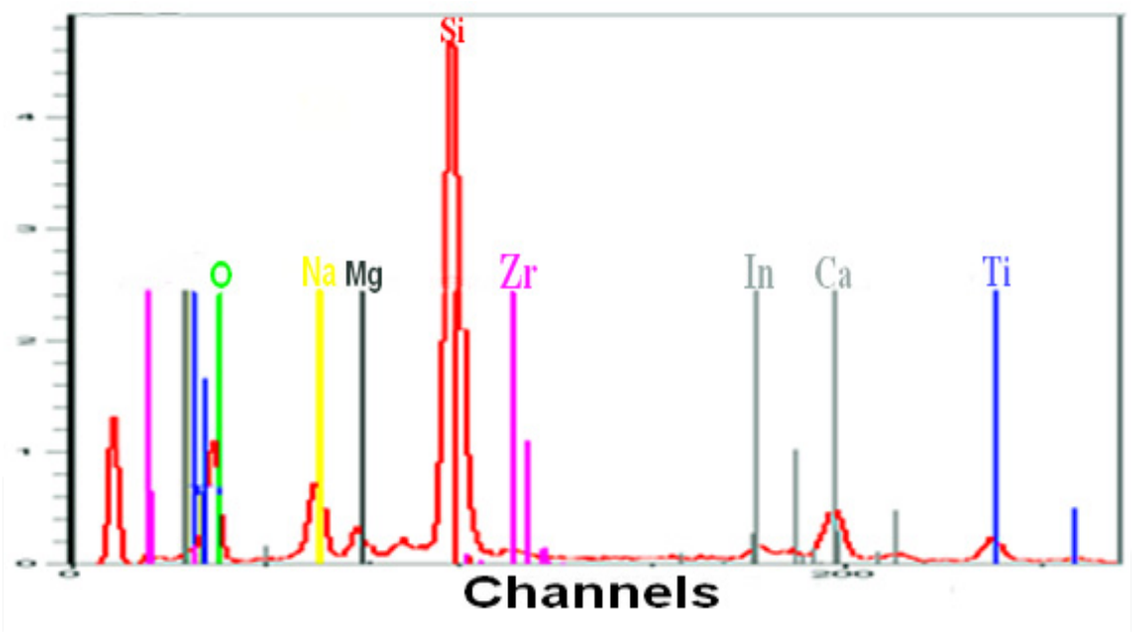

Figure 13. EDX spectra of 5% ZrO_2-doped TiO_2 thin films annealed at 450°C.

3.3.2. Optical properties

3.3.2.1. UV absorption analysis

Figure 14 display diffused scattering UV-VIS transmittance spectra of TiO_2 thin films undoped and 5% ZrO_2-doped TiO_2, for different annealing temperatures from 350°C to 450°C and different numbers of dipping (3, 4, 6, 8 dipping) in the wavelength range 300–800 nm, where the film due to interference phenomena between the wave fronts generated at

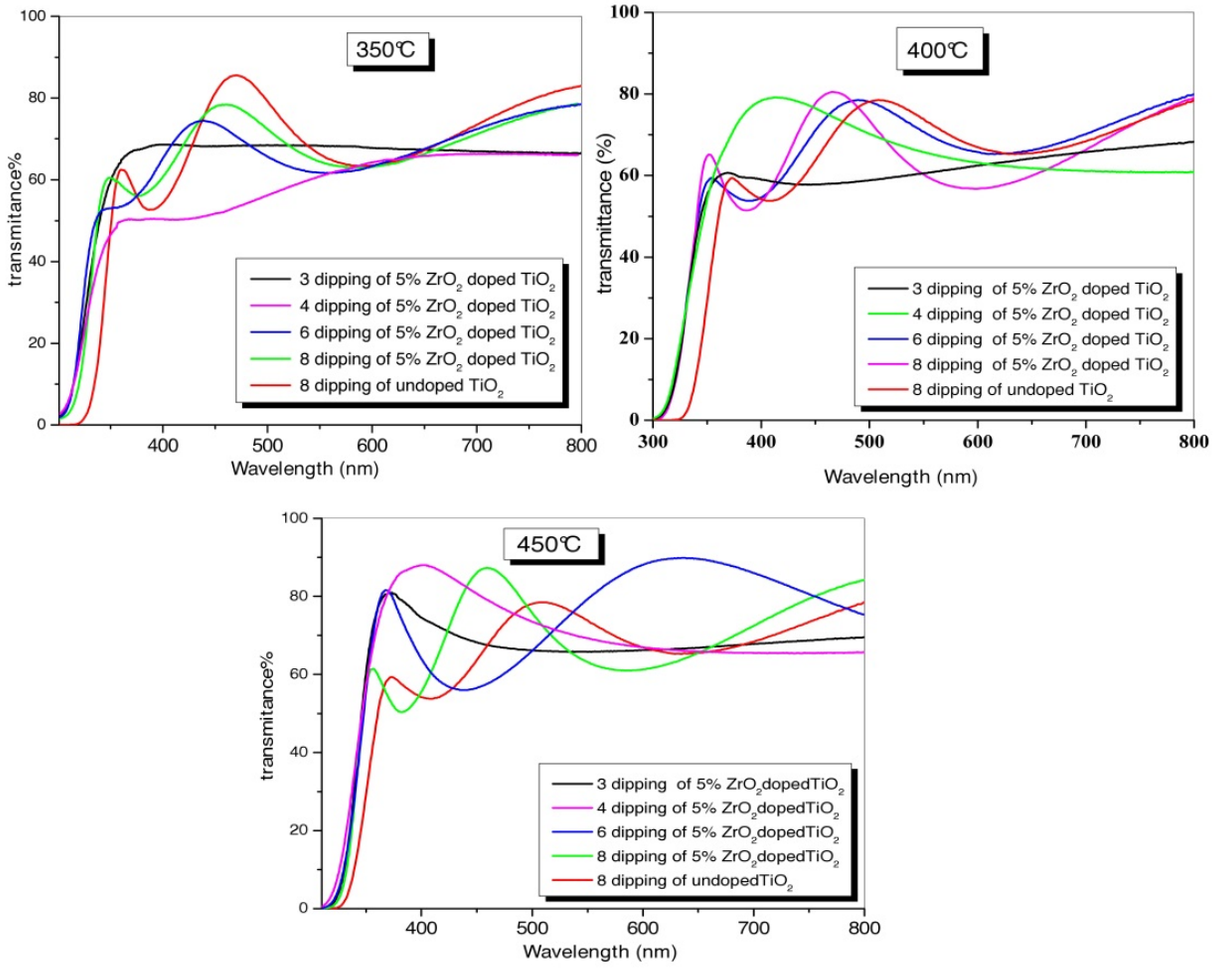

Figure 14. UV–VIS spectra of undoped TiO_2 and 5% ZrO_2-doped TiO_2 thin films, for various dipping and at different annealing temperatures.

the two interfaces (air and substrate) defines the sinusoidal behavior of the curves' transmittance versus wavelength of light. The curves showed a similar behavior in the temperature range:

- A **region** characterized by a strong absorption at $\lambda < 380$ nm, this absorption is due to the transition electronic inter-band.
- High transmittance region, from 60 to 95% on a wide range of wavelength in the visible region (from 380 to 800 nm) has been observed which may be used in applications in solar cells. High transparency is one of the most important properties that explain the interest in undoped or doped TiO_2 thin films.

As can be seen, all the spectrums exhibit interference fringes, which are due to the multiple reflections at the two film edges, i.e. at the film/air and the film/substrate interfaces. This indicates that the top film surface is smooth and uniform and exhibits a good transparency in the visible region. So that the excellent surface quality and homogeneity of the film were confirmed from the appearance of interference fringes in the transmission spectra. This occurs when the film surface is reflecting without much scattering/absorption in the bulk of the film.

If the film surface is rough, the radiation in film/air interface undergo scattering in all directions instead of a reflection. Oh et al. [28], Kim et al. [77] show that the interference fringes are due the increase in thin films thickness. The occurrence of such fringes means that our films are sufficiently thick

Analysis of UV– VIS transmission spectra shows that the 5% ZrO_2-doped TiO_2 thin films are transparent in the visible range and opaque in the UV region, whatever are the annealing temperature and number of dipping

The amplitude of interference spectra increased with increasing calcination temperature. These results show that the refractive index of TiO_2 thin films is increased while the film thickness is decreased. This can be due to the formation stage of anatase and with the increase in the grain size [28].

A slight shift of transmission curves to lower wavelengths is observed for curves of ZrO_2-doped thin films in comparison with those undoped (figure 14) This shift is ascribed to the increase in band gap energy.

3.3.2.2. Refractive index, density, thickness and porosity

The refractive index of TiO_2 thin films was calculated from measured UV–VIS transmittance spectrum. The evaluation method used in this work is based on the analysis of UV–VIS transmittance spectrum of a weakly absorbing film deposited on a non-absorbing substrate [78]. The refractive index n (λ) over the spectral range is calculated by using the envelopes that are fitted to the measured extreme:

$$n(\lambda) = \sqrt{S + \sqrt{S^2 - n_0^2(\lambda) n_S^2(\lambda)}}$$

$$S = \frac{1}{2}\left(n_0^2(\lambda) + n_S^2(\lambda)\right) + 2 n_0 n_S \frac{T_{\max}(\lambda) - T_{\min}(\lambda)}{T_{\max}(\lambda) \times T_{\min}(\lambda)}$$

Where n_0 is the refractive index of air, n_s is the refractive index of the film, T_{max} is the maximum envelope, and T_{min} is the minimum envelope. The thickness of the films was adjusted to provide the best fits to the measured spectra. In this study, all the deposited films are assumed to be homogeneous.

The porosity of the thin films is calculated using the following equation [79]

$$Porosité = \left(1 - \frac{n^2 - 1}{n_d^2 - 1}\right) \times 100(\%)$$

Where n_d is refractive index of pore-free anatase (n_d = 2.52) [80], and n is refractive index of porous thin films.

The relationship between density, and refractive index for the polymorphs was proposed by Gladstone-Dale [81]. This relationship is as follows:

$$n = 1 + 0,4\rho$$

Where :

n: mean index of refraction,
d: density
0,40: Gladstone-Dale constant for TiO_2
The thickness of the films was calculated using the equation:

$$d = \lambda_1\lambda_2/2\ (\lambda_1 n_2 - \lambda_2 n_1)$$

Where n_1 and n_2 are the refractive indices corresponding to the wavelengths λ_1 and λ_2, respectively [82].

The results of the computed refractive index (n) (figure 15), density (ρ) and porosity (p) (figure 16) are shown in Table 5. It is noted that the refractive index and the density of thin films of doped titanium oxide increases with increasing annealing temperature and number of dipping; due to phase transition (anatase, anatase–brookite), which increases grain sizes and/or the density of layers.

This phenomenon is related to crystallization, pores destruction and densification of associated film, as well as the elimination of organic compounds.

However, the porosity decreases with increasing annealing temperature and film thickness.

		4 Dipping			*6 Dipping*			*8 Dipping*		
T (°C)	***Films of***	***n***	***ρ***	***P(%)***	***n***	***ρ***	***P(%)***	***n***	***ρ***	***P(%)***
350°C	**TiO_2**	*1,92*	*2,30*	*49,8*	*2,15*	*2,88*	*36,3*	2,19	*2,98*	*29,1*
	TiO_2 : ZrO_2	*1,62*	*1,55*	*69,3*	*2,13*	*2,83*	*33,9*	*2,18*	*2,95*	*29,7*
400°C	**TiO_2**	*2,11*	*2,78*	*35,5*	*2,21*	*3,03*	*27,4*	*2,25*	*3,13*	*24,1*
	TiO_2 : ZrO_2	*1,91*	*2,28*	*50,3*	*2,18*	*2,95*	*29,9*	*2,21*	*3,03*	*27,4*
450°C	**TiO_2**	*2,15*	*2,88*	*36,3*	*2,29*	*3,23*	*20,7*	*2,37*	*3,43*	*13,7*
	TiO_2 : ZrO_2	*2,17*	*2,93*	*30,7*	*2,23*	*3,08*	*25,7*	*2,29*	*3,23*	*20,7*

Table 5. Variation of refractive index (n), density (ϱ), porosity (p) of undoped and 5% ZrO_2-doped TiO_2 for different annealing temperatures and different thickness.

The calculated values of thin films thickness are given in table 6. It is clearly observed that the film thickness increases with the number of dipping and annealing temperatures, which is in good agreement with results obtained previously of thickness determined with a surface profiler.

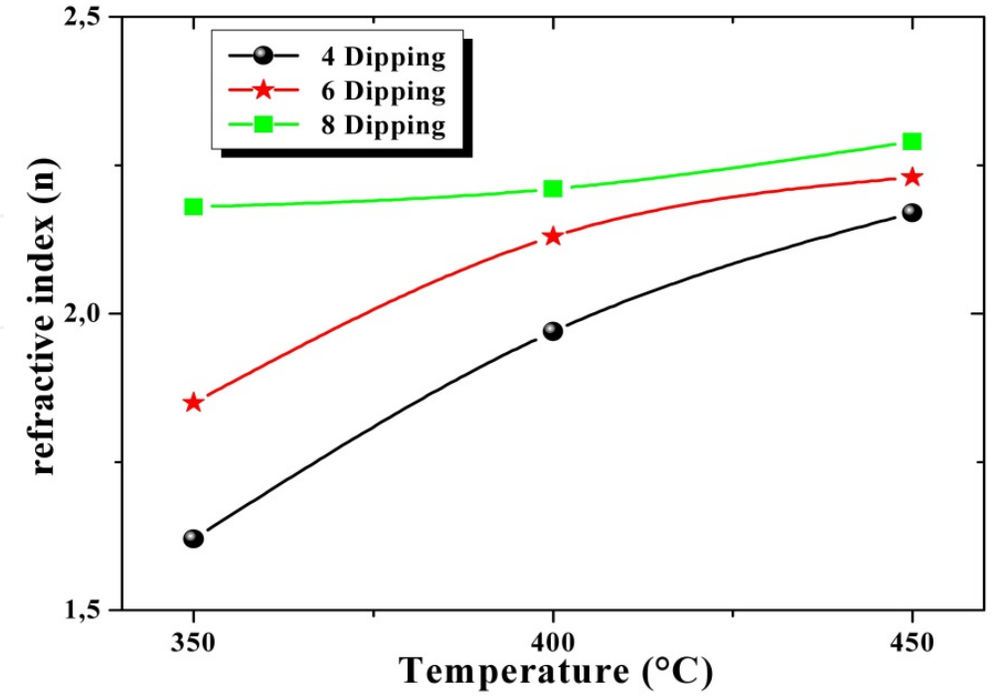

Figure 15. Variation of refractive index (n) of 5% ZrO_2-doped TiO_2 for different annealing temperatures and different thickness

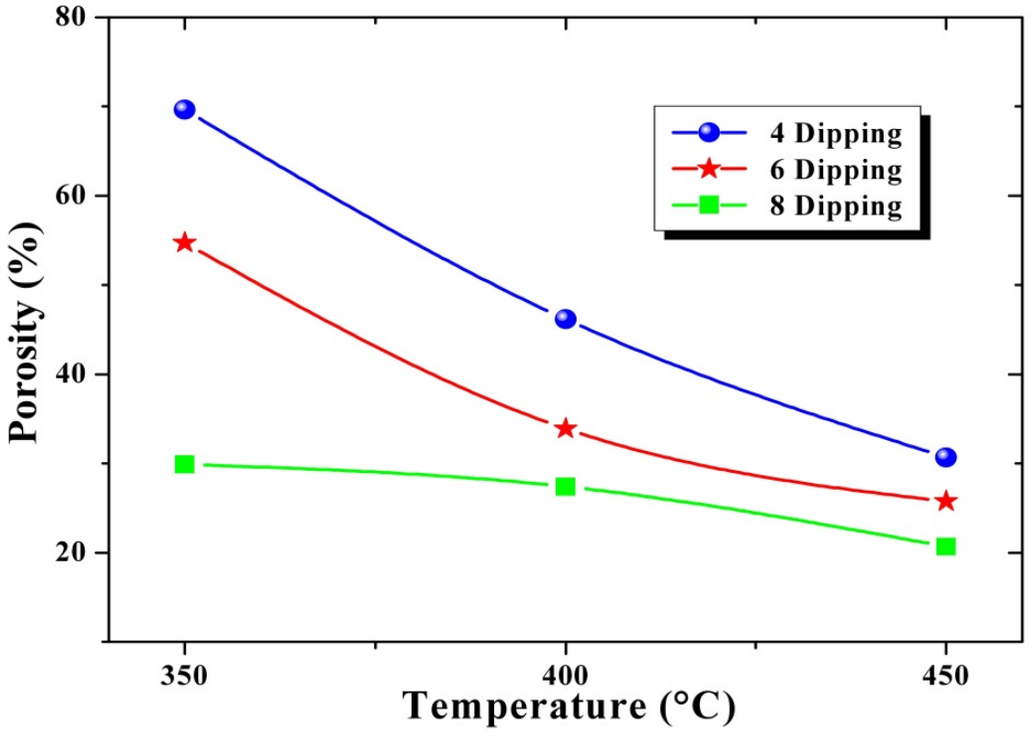

Figure 16. Variation of porosity (p) of 5% ZrO_2-doped TiO_2 for different annealing temperatures and different thickness.

	Thickness d (nm)		
T (°C)	***4 Dipping***	***6 Dipping***	***8 Dipping***
350°C	127	194	268
400°C	139	216	274
450°C	158	233	289

Table 6. Variation of calculated film thicknesses d (nm) for different annealing temperatures and different dipping.

3.3.2.3. Optical band gap:

The band gap is then found as the intercept of the linear portion of the plot. For a direct band gap semi-conductor, the absorption near the band edge can be estimated from the following equation known as the Tauc plot [83]:

$$(ah\nu) = C\left(h\nu - E_g\right)^n$$

Where C is a constant, E_g the optical band, α is the optical absorption coefficient, $h\nu$ is the photon energy gap, h the Plank's constant and the exponent n characterizes the nature of band transition; the values of n = 1/2 and 3/2 correspond to direct allowed and direct forbidden transitions, n = 2 and 3 are related to indirect allowed and indirect forbidden transitions [83] and in the cases for a direct band gap semi-conductor like TiO_2 the relation become [84, 85]:

$$(ah\nu)^2 = C\left(h\nu - E_g\right)$$

The energy band gap (E_g) of the films can be estimated by plotting $(\alpha h\nu)^2$ versus $h\nu$ (Figure 17), then extrapolating the straight-line part of the plot to the photon energy axis. The energy band gap of 5% ZrO_2-doped TiO_2 films, given in table 7, decrease owing to an increase in annealing temperatures and the number of dipping. The values are 3.65 and 3.54 eV at 350°C and 450°C respectively.

This decrease was correlated with grains size increases with temperature, when the latter increases the defects and impurities tend to disappear causing a reorganization of the structure. We find that doping with ZrO_2 causes an increase in the band gap by contrast to that of undoped TiO_2 (3.50 eV).

	Band gap (eV)			
T (°C)	***3 Dipping***	***4 Dipping***	***6 Dipping***	***8 Dipping***
350°C	3,79	3,74	3,71	3,65
400°C	3,73	3,70	3,68	3,59
450°C	3,67	3,63	3,61	3,54

Table 7. Variation of band gap of 5% ZrO_2-doped TiO_2 thin films for different annealing temperatures and different thickness.

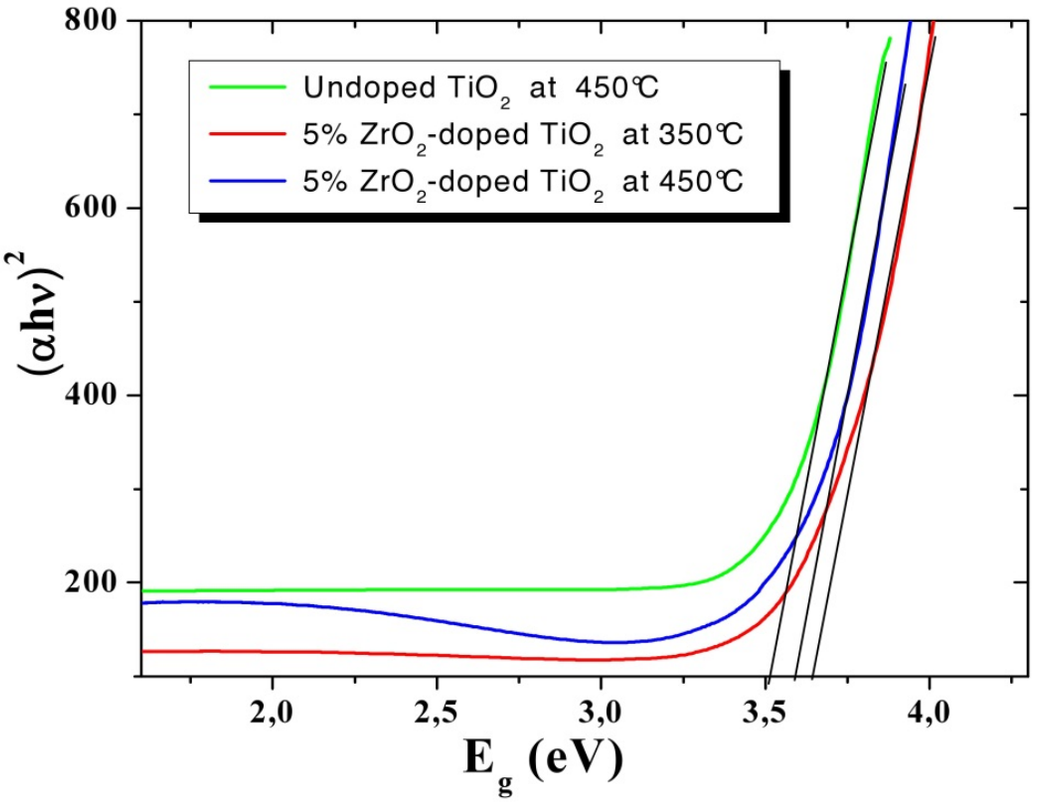

Figure 17. Plot of $(\alpha h\nu)^2$ versus $(h\nu)$ for determination of band gap of undoped and 5% ZrO_2-doped TiO_2.

4. Conclusion

In this study, we investigated the transformation behaviors and the effect; of a smaller ratio range of ZrO_2; doping on the surface area of TiO_2 thin films, band gap energy, variations of crystal granularity, phase composition and especially on the evolution of the crystallite size and defects concentration with annealing treatments and layers thickness of the samples produced. So that in this chapter, we report the study of structural, thermal and optical properties of ZrO_2-doped TiO_2 thin films deposited by the sol–gel process

Analyses of doped TiO_2 xerogel show that addition of 5% ZrO_2 would be largely sufficient to form nanoparticles of anatase (size of grain of 14.78 nm) by contrast to that of undoped TiO_2. X-ray diffraction and Raman spectroscopy analyses exhibit that doped thin films obtained starting from annealing at 350°C crystallize in both anatase and brookite phases. Calculation of grain sizes by Scherrer's formula, gives sizes ranging from 8.58 to 20.56 nm and we note an increase in grain sizes by increasing the annealing temperature for all structures. Raman spectroscopy studies confirms the results found by XRD and reveal that

the films annealed from 350 to 450◦C crystallizes in anatase and brookite structure. From the DSC analysis, we have demonstrated that an annealing temperature equal or higher than 340 °C for undoped and 260 ◦C for 5% ZrO_2-doped would be sufficient to form titanium oxide. The addition of 5% of zirconium oxide led to a shift of exothermic peak phase towards lower temperatures, due to the speeding up of the crystallization of titanium oxide compared to the undoped one.

Analysis of UV-VIS transmission spectra shows that the 5% ZrO_2-doped TiO_2 thin films are transparent in the visible range and opaque in the UV region, whatever the annealing temperature and the number of dipping. Refractive index of the thin films of titanium oxide increases with increasing annealing temperature and number of dipping, but the porosity decreases, due to phase transition (anatase, anatase–brookite), which increases grain sizes and/or density of layers. Energy band gap of 5% ZrO_2-doped TiO_2 films decrease owing to an increase in annealing temperatures, also we find that doping with ZrO_2 causes an increase in the band gap by contrast to that of undoped TiO_2.

The optical properties of the films are found to be closely related to the microstructure and crystallographic structure which depend on the annealing temperature. In summary, In this study, we successfully fabricated ZrO_2-doped TiO_2 thin films, with desired structural and optical properties by sol–gel dip coating using the titanium alkoxide (tetrabutyl-orthotitanate) as a starting material.

Author details

Rabah Bensaha and Hanene Bensouyad
Laboratory of ceramics, University of Constantine 1, Constantine, Algeria

5. References

[1] Hu L, Yoko T, Kozuka H, Sakka S (1992) Thin Solid Films j. 18: 219.
[2] Brinker C.J, Scherer G.W (1990) Sol–Gel Science, Academic Press, San Diego, CA.
[3] Brinker C.J, Frye G.L, Hurd A.J, Ashlet C.S (1991) Thin Solid Films j. 97: 201.
[4] Nishio K, Sei T, Tsuchiya T (1996a) Preparation and electrical properties of ITO thin films by dip-coating process. Mater. Sci. Tech. J. 31: 1761–1766
[5] Nishio K, Miyake S, Sei T, Watanabe Y, Tsuchiya T (1996b) Preparation of highly oriented thin film exhibiting transparent conduction by the sol–gel process. Mater. Sci. J. 31: 3651–3656
[6] Nishio K, Seki N, Thongrueng J, Watanabe Y, Tsuchiya T (1999a) Preparation and properties of highly oriented thin films by a sol–gel process. Sol–Gel Sci. Tech J. 16: 37–45

[7] Nishio K, Kudo C, Nagahama T, Manabe T, Yamaguchi I, Watanabe Y, Tsuchiya T (2000b) Preparation and characterzation of epitaxial thin films prepared by sol–gel process. Mater. Res. Soc. J. 623: 377–382
[8] Nishio K, Watanabe Y, Tsuchiya T (2003) Epitaxial growth of thin films prepared from sol–gel process. Sol–Gel Sci. Tech. J. 26: 245–250
[9] Kodaira T, Nishio K, Yamaguchi I, Suzuki S, Tsukada K, Tsuchiya T (2003) Synthesis and properties of highly conductive thin films as buffer layer from sol–gel process. Sol–Gel Sci. Tech. J. 26: 1049–1053
[10] Larson S.A, Falconer J.L (1994) Appl. Catal. B: Environ. j. 4: 149.
[11] Pas Y, Heller A (1997) Mater. Res. J. 12: 2759.
[12] Hara K, T. Hariguchi, T. Kinoshita, K. Sayama, H. Arakawa, Solar Energy Mater. Solar Cell. 70 (2001) 151.
[13] Sakha V.A, Arabatzis I.M, Konstantinou I.K, Dimou A.D, Albanis T.A, Falaras P (2004) Appl. Catal. B: Environ. J. 49: 195.
[14] Tachibana Y, Ohsaki H, Hayashi A, Mitsui A, Hayashi Y (2000) Vacuum j. 59: 836.
[15] Zheng S.K, Wang T.M, Xiang G, Wang C (2001) Vacuum j. 62: 361.
[16] Radecka M, Zakrzewska K, Czternastek H, Stapinéski T, Debrus S (1993) Appl. Surf. Sci. j. 65: 227.
[17] Dumitriu D, Bally A.R, Ballif C, Hones P, Schmid P.E, Sanjinés R, Lévy F, Pârvulescu V.I (2000) Appl. Catal. B: Environ. J. 25: 83.
[18] Takeda S, Suzuki S, Odaka H (2001) Thin Solid Films j. 392: 338.
[19] Zhang F, Huang N, Yang P (1996) Surf. Coat. Technol. J. 84: 476.
[20] Aidla A, Uustare T, Kiisler A.A, Aarik J, Sammelselg V (1997) Thin Solid Films j. 305: 270.
[21] Abou-Helal M.O, Seeber W.T (2002) Appl. Surf. Sci. j. 195: 53.
[22] Choi Y, Yamamoto S, Umebayashi T, Yoshikawa M (2004) Solid State Ionics j. 172: 105.
[23] Hu L, Yoko T, Kozuka H (1992) Thin Solid Films j. 219: 18.
[24] Chrysicopoulou P, Davazoglou D, Trapalis C, Kordas G (1998) Thin Solid Films j. 323: 188.
[25] Kim D.J, Hahn S.H, Oh S.H, Kim E.J (2002) Mater. Lett. j. 57: 355.
[26] Yang J, Li D, Wang H, Wang X, Yang X, Lu L (2001) Mater. Lett. j. 50: 230.
[27] Huber B, Brodyanski A, Scheib M, Orendorz A, Ziegler C, Gnaser H (2005) Thin Solid Films j. 472: 114.
[28] Oh S.H, Kim D.J, Hahn S.H, Kim E.J (2003) Mater. Lett. j. 57: 4151.
[29] Wang C, Xu BQ, Wang XM, Zhao JC (2005) Solid State Chem J. 178:3500.
[30] Hu C, Tang YC, Yu JC, Wong PK (2003) J photocatalyst Appl Catal B Environ 40:131.
[31] Bensouyad H, Sedrati H, Dehdouh H, Brahimi M, Abbas F, Akkari H, Bensaha R (2010) Thin Solid Films J. 519:96.
[32] Yang J, Li D, Wang X, Yang XJ, Lu LD (2002) J Solid State Chem 165:193.

[33] Li JL, Liu L, Yu Y, Tang YW, Li HL, Du FP (2004) Electrochem Commun J. 6:940.
[34] Bandara J, Hadapangoda CC, Jayasekera WG (2004) J Appl Catal B Environ 50:83.
[35] Li XZ, Li FB, Yang CL, Ge WK (2001) Photochem Photobiol A Chem J. 141:209.
[36] Shchukin D, Poznyak S, Kulak A, Pichat P (2004) Photochem Photobiol A Chem J. 162:423.
[37] Bensouyad H, Adnane D, Dehdouh H, Toubal B, Brahimi M, Sedrati H, Bensaha R (2011) *Sol-Gel Sci Technol J.* 59: 546.
[38] Takahashi YK, Ngaotrakanwiwat P, Tatsuma T (2004) photocatalysts Electrochim Acta J. 49: 2025.
[39] Wu L, Yu JC, Fu XZ (2006) Mol Catal A Chem J. 244:25.
[40] Su H, Xie Y, Gao P, Xiong Y, Qian Y (2001) J Mater Chem 11:684.
[41] Zelner M, Minti H, Reisfeld R, Cohen H, Tenne R (1997) Preparation and characterization of CdS films synthesized in situ in zirconia sol-gel matrix, Chem. Mater. J. 9: 2541.
[42] Sashchiuk A, Lifshitz E, Reisfeld R, Saraidarov T, Zelner M, Willenz A (2001) Optical and conductivity properties of PbS nanocrystals in amorphous Zirconia sol-gel films, of Sol-Gel Science and Technology J. 24: 31.
[43] Wang M.T, Wang T.H, Lee J (2005) Electrical conduction mechanism in high-dielectric-constant ZrO2 thin films, Microelecton. Reliability j. 45: 969.
[44] Harrison H.D.E, McLamed N.T, Subbaro E.C (1963) A new family of self-activated phosphors, Electrochem. Soc J. 110: 23.
[45] Lowdermilk W.H, Milam D, Rainer F (1980) Optical coatings for laser fusion applications, Thin Solid Films j. 73: 155.
[46] Meier S.M, Gupta D.K (1994) The evolution of thermal barrier coatings in gas turbine engine applications, Eng. Gas Turbines Power Trans. ASME J. 116: 250.
[47] Wendel H, Holzschuh H, Suhr H, Erker G, Dehnicke S, Mena M (1990) Thin zirconium dioxide and yttrium oxide-stabilized zirconium dioxide films prepared by plasma-CVD, Mod. Phys. Lett. B j. 4: 1215.
[48] Fork D.K, Fenner D.B, Connell G.A.N, Phillips J.M, Geballe T.H (1990) Epitaxial yttria-stabilized zirconia on hydrogen-terminated Si by pulsed laser deposition, Appl. Phys. Lett. j. 57: 1137.
[49] Patel A.M, Spector M (1997) Tribological evaluation of oxidized zirconium using an articular cartilage counterface: a novel material for potential use in hemiarthroplasty, Biomaterials j. 18: 441.
[50] Balamurugan A, Kannan S, Rajeswari S (2003) Structural and electrochemical behaviour of sol-gel zirconia films on 316L stainless-steel in simulated body fluid environment, Mater. Lett. j. 57: 4202.
[51] Ritala M, Leskela M (1994) Zirconium dioxide thin films deposited by ALE using zirconium tetrachloride as precursor, Appl. Surf. Sci. j. 75: 333.
[52] Cao G.Z, Brinkman H.W, Meijerink J, De Vries K.J, Burgraaf A.J (1993) Pore narrowing and formation of ultrathin yttria-stabilized zirconia layers in ceramic membranes by

chemical vapor deposition/electrochemical vapor deposition, Am. Ceram. Society. J. 76: 2201.
[53] Emeline A, Kataeva G.V, Litke A.S, Rudakova A.V, Serpone N (1998) Langmuir j. 14: 5011.
[54] Mechiakh R, Bensaha R (2006) C.R. Phys j. 7: 464.
[55] Ivanda M, Music S, Popovic S, Gotic M (1999) J Mol Struct 480: 645.
[56] Kitiyanan A, Yoshikawa S (2005) Materials Letters J. 59: 4038.
[57] Neppolian B (2007) Applied Catalysis A: General j. 333: 264.
[58] Pérez-Hernandez R, Gomez-Cortes A, Arenas-Alatorre J, Rojas S, Mariscal R, Fierro J.L.G, Diaz G (2005) Catal. Today j. 107: 149.
[59] Perdew J.P, Wang Y (1992) Phys. Rev. B j. 45: 13244.
[60] Montoya I.A, Viveros T, Dominguez J.M, Channels L.A, Schifter I (1992) Catal. Lett. J. 15: 207.
[61] Mechiakh R, Meriche F, Kremer R, Bensaha R, Boudine B, Boudrioua A (2007) Opt. Mater. J. 30: 645.
[62] Landau L.D, Levich B (1942) Acta Physicochim. J. 17: 42.
[63] Michels A. F, Manegotto T, Horowitz F (2004) Appl. Opt. j. 43: 820.
[64] Hewak D. W, Lit J. W. Y (1988) Can. J. Phys, 66: 861.
[65] Cullity B.D (1978) Elements of X-Ray Diffraction, 2nd ed.Addison-Wesley, Reading, MA.
[66] Ray S, Banerjee R, Baraua A.K (1980) Jpn J. of Appl Phys 19:1889.
[67] Yang H, Huang C, Tang A, Zhang X, Yang W, *Materials Research Bulletin,* 40 (2005) 1690.
[68] Lottici P.P, Bersani D, Braghini M, Montenero A (1993) Mater. Sci. J. 28: 177.
[69] Djaoued Y, Badilescu S, Ashrit, Bersani D, Lottici P.P, Robichaud J (2002) *Sol-Gel Sci Technol J.* 24: 255.
[70] Liao M.H, Hsu C.H, Chen D.H (2006) J Solid State Chem 179: 2020.
[71] Xie Y, Liu X, Huang A, Ding C, Chu P.K (2005) J Biomaterials 26: 6129.
[72] McDevitt N.T, Baun W.L (1964) J Spectrochim Acta 20: 799.
[73] Music S, Gotic M, Ivanda M, Popovic S, Turkovic A, Trojko R, Sekulic A, Furic K (1997) Mater Sci Eng B 47: 33.
[74] Ocana M, Fornes V, Serna J.V (1988) J Solid State Chem 75: 364.
[75] Djaoued Y, Badilescu S, Ashrit P.V (2002) *Sol-Gel Sci Technol J.* 24: 247.
[76] Tian J (2009) Surface & Coatings Technology j. 204: 723.
[77] Kim S, Yum J, Sung Y (2005) Photochem Photobiol A: Chem J. 171: 269.
[78] Manifacier J.C, Gasiot J, Fillard J.P (1976) Phys. E J. 9: 1002.
[79] Yoldas B.E, Partlow P.W (1985) Thin Solid Films j. 129: 1.
[80] Kingery W.D, Bowen H.K, Uhlmann D.R (1976) Introduction to Ceramics, Wiley, New York.
[81] Gladstone, Dale (1863), Phil. Trans. J. 153: 317
[82] Swanepoel R (1983) Phys. E: Sci. Instrum. J. 16: 1214.

[83] Pankove J.I (1971) *Optical Process in Semiconductors*; Prentice Hall; Englewood; Cliffs; NJ; 34. p.
[84] Zhao X. K, Fendler J. H (1991) Phys. Chem. J. 95: 3716.
[85] Tang H, Prasad K, Sanjines R, Schimid P.E, Levy F (1994) App. Phys. J. 75: 2042.

IntechOpen